Wong, T.; Behl, M.; Yusoff, N.; Li, T.; Wahit, M.; Ismail, A.; Zhao, Q.; Lendlein, A.:

Bio-based composites from plant based precursors and hydroxyapatite with shape-memory capability.

In: Composites Science and Technology. Vol. 194 (2020) 108138.

First published online by Elsevier: 21.03.2020

https://dx.doi.org/10.1016/j.compscitech.2020.108138

Bio-based Composites from Plant Based Precursors and Hydroxyapatite with Shape-Memory Capability

Tuck-Whye Wong,[a,d,#] Marc Behl,[b,#] Noor Izyan Syazana Mohd Yusoff,[c] Tiefeng Li,[a,*] Mat Uzir Wahit,[c,*] Ahmad Fauzi Ismail,[d] Qian Zhao,[e] and Andreas Lendlein[b]

[a] Department of Engineering Mechanics, Zhejiang University, Hangzhou 310027, China

[b] Institute of Biomaterial Science and Berlin-Brandenburg Center for Regenerative Therapies, Helmholtz-Zentrum Geesthacht, Kantstr. 55, 14513 Teltow, Germany

[c] Center for Composite, Institute of Vehicle System and Engineering, Universiti Teknologi Malaysia, 81310 Skudai, Johor, Malaysia

[d] Advanced Membrane Technology Research Centre, Universiti Teknologi Malaysia, 81310 Skudai, Johor, Malaysia

[e] State Key Laboratory of Chemical Engineering, College of Chemical and Biological Engineering, Zhejiang University, Hangzhou 310027, China

KEYWORDS

Particle-reinforced Composites; Hybrid Composites; Smart Materials; Curing; Environmental Degradation

AUTHOR INFORMATION

[#] These authors contributed equally to this work.

* corresponding author: Prof. Dr. Tiefeng Li, Email: litiefeng@zju.edu.cn

* corresponding author: Prof. Dr. Mat Uzir Wahit, Email: r-uzir@utm.my

ABSTRACT

A series of bio-based composites consisting of degradable thermoset poly[xylitol-(1,12-dodecanedioate)] (PXD) and hydroxyapatite microparticles (HA) was prepared. Equimolar amounts of xylitol and 1,12-dodecanedioic acid were reacted under catalyst-free polyesterification and the synthesized composites (PXDHC*y*) consist HA particles ranging between 0 wt% and 20 wt%. Crystallinity of the polymer matrix decreased at low content of HA (5 wt%) as the microparticles hindered crystallization of 1,12-dodecanedioate segment and then increased when the content of HA was raised (from 10 wt% to 20 wt%) as the polymer chains crystallized on surface of microparticles. All PXD and PXDHC*y* are able to hydrolytically degrade with around 7 wt% to 20 wt% mass loss after 16 weeks incubation in water (rate depends on HA content). The capability of PXD and PXDHC*y* composites to keep a temporary shape after a deformation process correlated with the polymer crystallinity whereas the shape recovery was 99 %. The switching temperatures of PXD and PXDHC*y* composites ranged around 50 °C (and correlated to the melting-transition temperature) and did not vary with the loading of HA. A prototype of PXDHC*y* composite smart fixation plug was demonstrated and showed excellent potential to be used as bio-based fixation device for household appliances.

1. Introduction

Xylitol is a naturally occurring sugar alcohol, abundant in fruit and vegetable fibers [1]. Currently, the main source of commercial xylitol is extracted and processed from corn-cobs that require 5 months to grow and therefore can be considered as sustainable and environmentally friendly. Although 1,12-dodecanedioic acid (DA) is currently synthesized in an industrial scale from petroleum-based butadiene, it also can be obtained by omega-oxidation of lauric acid as well as oxidation from oil of *Vernonia galamensis* (seed oil of a plant species) [2-4]. Yeast has been established as a low cost and sustainable source for cost-effective production of DA. At present,

DA is mainly used in the production of nylon, paint-pigment, adhesive, and powder coating. Parallel to the raised demand for bio-based products, numerous chemical manufacturers are exploring bio-based synthesis-routes to synthesize DA.

In the past decade, a huge number of bio-based polymers were successfully synthesized utilizing renewable natural resources, with feedstock from plant oil [5-8], sugar [9,10], starch [11], carbohydrate [12,13], and lignin [14,15]. Exploitation of aforementioned biomasses for non-food and non-feed applications proved the idea of bio-based derived polymers [16]. The challenge that most bio-based polymers have a low Young's modulus as compared to petroleum-based polymers can be addressed by the incorporation of inorganic fillers or natural fibers into these bio-based polymers to enhance mechanical performance, electrical conductivity or magnetic properties. For example, hydroxyapatite (HA) has been incorporated within citric acid-based polyester in order to enhance the Young's modulus [17]. HA was shown to be an environmental friendly filler as it can be obtained from wastes [18-20].

Shape-memory polymers (SMPs) are polymeric materials with the capability to change shape in a programmable manner. SMPs are capable of being fixed in one or more temporary shapes and only recover the permanent shape when exposed to specific stimuli, typically "heat" [21]. The shape-memory effect of polymers has been applied in commercial products as early as the 1960s in the form of heat shrinkable polyethylene tubes, which are used as wire wraps for the purpose of electrical insulation [22]. It was also demonstrated that SMPs show significant potential in application fields ranging e.g. from aerospace, biomedicine, environment, and soft robotics [23-25]. Interestingly, few examples of shape-memory properties of bio-based polymers have been studied [26-28].

In this work, it was explored whether SMPs can be created by the reaction of xylitol with 1,12-dodecanedioic acid to form a bio-based SMP, namely poly[xylitol-(1,12-dodecanedioate)]

(PXD) network. PXD is a semi-crystalline thermoset, in which xylitol acts as net points while 1,12-dodecanedioic acid links the net points (crystallizable segment) (Scheme 1). In addition, it was investigated whether the mechanical, structural, thermal, and hydrolytic degradation properties of this biobased matrix material can be tailored by the incorporation of hydroxyapatite in different loadings into PXD matrix. Shape-memory properties of PXDHC*y* composites were quantified. Lastly, the bio-based composite demonstrated in a prototype smart fixation plug could potentially be used for numerous fixation purposes. Notably, low switching temperature (around 50 °C) of PXDHC*y* may seem more user-friendly.

Scheme 1 Synthesis of poly [xylitol-(1,12-dodecanedioate)] (PXD) network

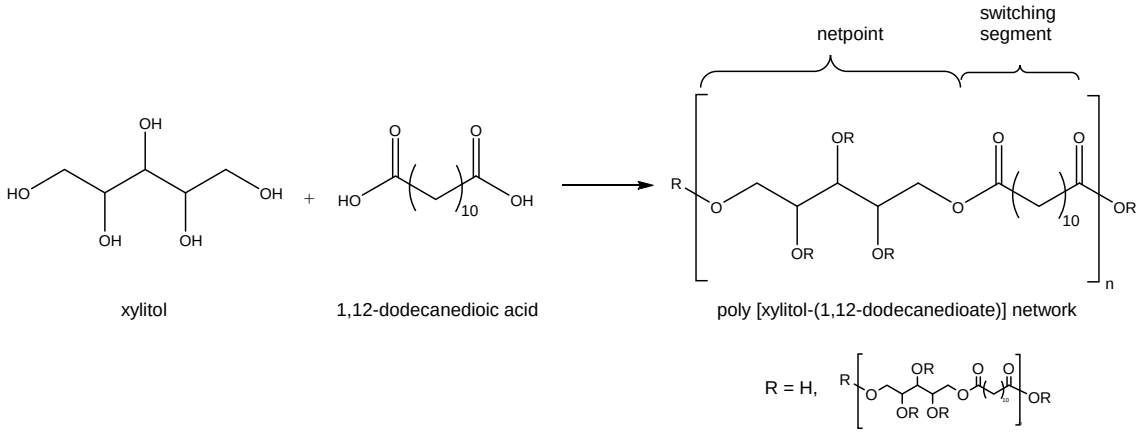

2. Experimental

2.1 Materials

HA [M_w = 502.32 g·mol^{-1}; particle size: <45 μm (98.1%), 45-75 μm (1.4%), >75 μm (0.5%)], tetrahydrofuran (>99%), xylitol (>99%), and 1,12-dodecanedioic acid (>99%) were purchased from Sigma Aldrich (Kuala Lumpur, Malaysia) and used as received.

2.2 Synthesis of PXD and PXDHC bio-based composites

Xylitol and 1,12-dodecanedioic acid were melted simultaneously in equimolar amounts at 165 °C in a reaction flask purged with nitrogen. When all monomers were completely melted, HA (0, 5, 10, 15, and 20 wt%) was added. The temperature of the heating bath was lowered to 155 °C

followed by a vigorous stirring at 250-300 rpm for 5 h. Afterwards the obtained mixture was cured by another polycondensation step at 140 °C for 48 h to yield the composites. The final composites were named PXDHC*y*, in which *y* denotes the HA content of the starting mixture.

2.3 Characterization and testing

FTIR: Infrared spectra of samples were obtained with NICOLET IS10-IR Spectrometer (FTIR). The spectrum was collected at the average of 32 scans with a signal resolution of 4 cm^{-1} within the range of 400 to 4000 cm^{-1}.

Swelling in Tetrahydrofuran (THF): Initial mass of the sample (1 cm × 1 cm, about 1-2 mm thickness) was recorded (W_o). Then the sample was placed in a beaker containing 20 mL of THF and swollen for 48 h at 22 °C. After this time period the THF swollen sample was quickly placed inside a small sampling bottle, its weight was recorded (W_{sw}), and then allowed to dry in an oven at 60 °C until constant mass was obtained (W_d). Final mass of sample was determined again. For each composition, five individual experiments were conducted. Gel content (G) and degree of swelling (Q) were calculated by using following equations: $\mathrm{G}\,(\%) = \frac{W_d}{W_o} \times 100\%$ and $\mathrm{Q}(\%) = \left[1 + \rho_2\left(\frac{W_{sw}}{W_d \times \rho_1} - \frac{1}{\rho_1}\right)\right] \times 100\%$, where ρ_1 and ρ_2 are the specific densities of the THF and sample film, respectively.

WAXD: Wide angle X-ray diffraction (WAXD) analyses were conducted by means of a Rigaku Diffractometer using Cu-Kα radiation (λ = 0.154 nm) with an accelerating voltage of 40 kV and a current of 30 mA, from 2θ = 5–60° with step sizes of 0.02° at 20 °C.

DSC: Differential scanning calorimetric (DSC) thermograms were recorded under nitrogen atmosphere using a DSC-820 (Mettler Toledo). First, the sample was heated from room temperature to 120 °C and then cooled down to -50 °C, followed by a second heating to 120 °C. Both the heating and cooling rates were fixed at 10 °C·min^{-1}

Mechanical testing: Tensile tests from which the elongation at break ε_p were determined with a Universal tester (Instron) from dumbbell-shaped samples (thickness around 1.5 mm) as according to ASTM D412-98a with a speed of 10 mm·min^{-1} at 25 °C and 70 °C. Five individual experiments were performed for each composition and temperature. The network strand density, ν (in units of moles of strand per unit volume of polymer) was calculated from the affine theory of rubber elasticity: $E = 3\nu RT\ (1 + 2.5\Phi + \Phi^2)$, where E is Young's modulus, R is universal gas constant, T is temperature, and Φ is volume fraction of particulate filler [29].

Investigation of morphology: Tensile-fractured surfaces of the PXDHC*y* composites were analyzed by Field Emission Scanning Electron Microscope (FESEM, Zeiss) at an accelerating potential difference of 3-15 kV in a secondary electron mode. Each sample was put under strain until breakage and uniformly coated with a thin layer of gold by a sputter coater (JFC-1200 Finer Coater, Jeol). The distribution of hydroxyapatite (HA) particles within a composite matrix was observed by using an Energy Dispersion Spectroscope (EDS, Oxford Instrument). Particle mapping sensitive to carbon, oxygen, calcium, and phosphate atoms was performed on the same specimens as used for FESEM photography.

Hydrolytic degradation test: Environmental degradation properties of PXD and PXDHC*y* composites were determined by quantification the mass loss of samples (1 cm × 1 cm, about 1-2 mm thickness) after incubation in 50 mL distilled water at room temperature (22 °C). The incubation medium was refreshed every 7 d to prevent saturation. After each time interval, the sample was taken out, washed with distilled water followed by drying for 4 d at 60 °C. Five individual experiments were performed for each of the formulations at each time point. The final result was the averaged value. The weighing and drying processes were repeated until a constant mass was obtained.

Thermocyclic mechanical analysis: Shape-memory properties of PXD and PXDHC*y* composites were quantified in cyclic, thermomechanical tests with a Microforce Tester Instron 8848 under strain-controlled programming and stress-free recovery conditions. The tests consisted of four steps: (1) stretching the samples to ε_1 = 50% under tensile load at T_{high} = 70 °C, (2) cooling to T_{low} = 10 °C while ε_1 was kept constant, (3) release of stress at T_{low}, keeping this temperature for 10 min, and afterwards (4) heating to 70 °C. From the strain-stress curve, maximum strain during shape programming (ε_1), strain in stress free condition (ε_2), and the residual strain after shape recovery (ε_3) were obtained. The cycle was repeated 5 times from which the shape-fixity ratio (R_f) and shape-recovery ratio (R_r) were calculated by using following equations: $R_f = \frac{\varepsilon_2(N)}{\varepsilon_1} \times 100\%$ and $R_r = \frac{\varepsilon_1 - \varepsilon_3(N)}{\varepsilon_1 - \varepsilon_3(N-1)} \times 100\%$, where N denoted the N^{th} cycle [30]. Please note that elongation at break of PXDHC0 at 70 °C is around 12% and thus, the ε_1 during step (1) for PXDHC0 was set to 10%.

Statistical analysis: Data are expressed as mean ± standard deviation. The statistical significance between two sets of data was calculated using two-tail Student's t-test. Data were taken to be significant, when a P-value of 0.05 or less was obtained.

3. Result and discussion

PXDHC*y* composites with HA contents between 0 wt% and 20 wt% were prepared according to the procedure described in the experimental part. Experimentally, it was found that formulation with 25 wt% of HA was too brittle to handle and thus, this research work only focuses on synthesis, characterization, and testing of composites with HA percentage of (5 wt% to 20 wt%). Besides, PXDHC*y* was found to be difficult to gel at temperatures lower than 140 °C and also, the value of gel content did not change much even when the polycondensation step was extended for an additional 24 h. FTIR spectra PXDHC*y* composites with HA as well as PXD for reference are shown in Fig. 1. The bands at 1737 cm^{-1} (C=O) and 1080 cm^{-1} (C-O), which can be

assigned to ester bonds, were determined in all spectra of PXD and composites [31]. Compared to neat HA and PXD, no new bands were observed in the FTIR spectra of the composites, indicating no significant chemical interaction between PXD and HA. However, all bands were slightly shifted when compared to the spectra from the neat polymer PXD and the HA filler with composites that may be explained by the interaction of HA with the hydrogen-bonds of PXD. Presence of HA might influence the chain length between net points. Similar IR spectra of thermally crosslinked polyesters/inorganic filler composites were reported [32].

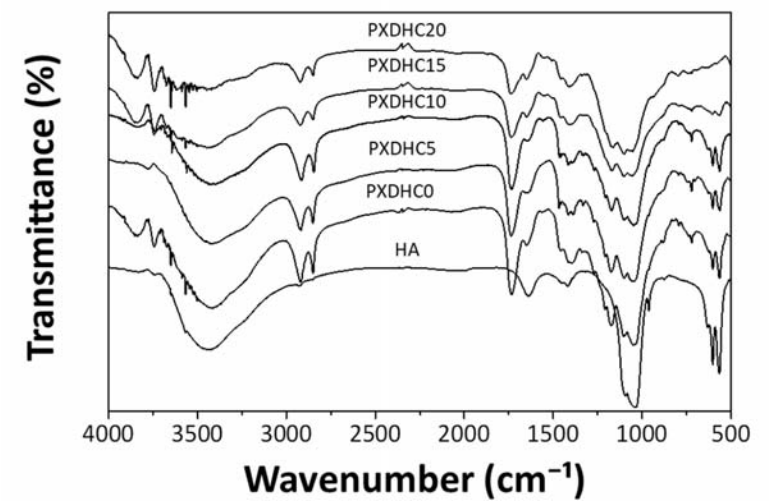

Fig. 1. FTIR spectra of PXD, HA, and PXDHC*y* composites

Gel content of PXD and PXDHC*y* are recorded in Table 1. After being incubated in THF, approximately 24 wt% of the PXD matrix was extracted, indicating the gelation of PXD achieved around 76 wt%. It was found that the percentage of gelation remained unchanged even when the duration of curing exceeded 72 h, which may be attributed to the increase in steric hindrance caused by the dense xylitol based crosslinks or the increase of viscosity. HA is an inorganic compound soluble in water neither nor THF. By taking the insolubility properties of HA as basis, a theoretical gel content curve was drawn for each formulation of PXDHC*y* composites (Fig. 2A). Although gel content of PXDHC*y* composite was expected to increase with higher loading of HA,

all the experimental values were lower than that of theoretical values. There is a considerably deviation between experimental results with theoretical values.

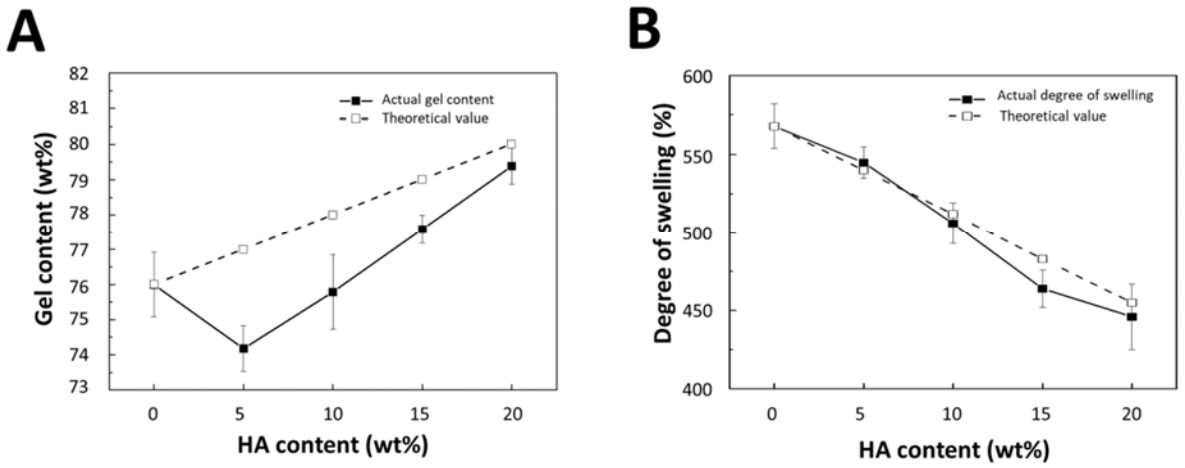

Fig. 2. (A) Gel content of PXD and PXDHC*y* composites and (B) Swelling degree of PXD and PXDHC*y* composites. Solid cubes connected with solid lines are the actual experimental results. Hollow cubes connected with dash lines are the theoretically calculated value.

In PXDHC*y* composites matrix, HA act as foreign particles this might block the PXDHC*y* polymer chains from crosslinking during thermal curing. As a result, the gelation ability of PXDHC*y* pre-polymer was reduced. Although experimental values were lower than that of the theoretical values, the deviations between actual values and theoretical values were found to be smaller with increasing amount of HA. It was found that the addition of HA into PXDHC*y* matrix showed two counteracting effects: For PXDHC*y* composite with low loading of HA, the crosslinking ability of PXDHC*y* matrix was restricted due to the presence of HA particles resulting in a reduction in gel content. As loading of HA increased, PXDHC*y* matrix may force to form a physical interaction with HA particles, which could be realized by unreacted hydroxyl groups. Although the gel content was still lower than the theoretically calculated value, the deviations could be reduced. The finding about existence of interaction between HA and PXDHC*y* matrix

was proved by WAXD pattern and DSC thermogram analysis, which are discussed in the next section.

Fig. 2B displays swelling degree of PXD and PXDHC*y* composites by incubation in THF. HA does not contribute to the swelling ability. Thus, the degree of swelling depends on the polymer-solvent interaction which, as expected, the swelling degree of PXDHC*y* decreased gradually with loading of HA. Degrees of swelling of sample with 0 wt%, 5 wt%, 10 wt%, 15 wt%, and 20 wt% of HA are about 568%, 545%, 506%, 464%, and 446% respectively. Theoretical degree of swelling of PXDHC*y* composites were calculated based on the assumption that HA is not soluble or swell in THF.

It was found that experimental values of swelling degree are slightly deviated from the calculated theoretical values. For composites with low loading HA, presence of HA particles will hinder the crosslinking capability of polymer network leading to lower gel content and higher degree of swelling. As loading of HA increased, the interaction between HA particles with PXDD matrix will become better and thus, some of the PXD chains had been absorbed on the particles surface and limit from swelling in THF. As a result, composites with a higher loading of HA showed a lower degree of swelling. In referring to sol-gel analysis, the effects of addition HA particles within PXD matrix could be shown in two different ways. Inorganic and organic materials do not show direct chemical interaction. Thus, the shielding effect of HA particles on crosslinking capability of PXD matrix is under prediction. However, extra hydroxyl groups due to non-equal starting materials possibly induce physical interaction between HA particles and PXD matrix. It can be concluded that there is competition between two counteracting factors in accordance to the analysis.

Influence of the HA on the crystallinity of the PXDHC*y* composites was investigated by means of WAXD. Fig. 3A and Fig. 3B show WAXD patterns of PXD and PXDHC*y* composites

before- and after extraction, respectively. The diffraction peaks of HA, which can be assigned to each of the planes as marked in its pattern (Fig. 3C) in accordance to ICPDS files HA [33], are present in all PXDHC*y* composites. In the diffraction patterns, position of HA peaks in all PXDHC*y* composites remain almost constant regardless of HA content, indicating that physical blending of HA particles with pre-polymer of PXD does not alter crystalline structure of HA [34,35]. The PXD is a semi-crystalline polymer which provides a sharp and characteristic diffraction peak at $2\theta = 21°$ attributed to the crystalline segments from 1,12-dodecanedioic acid as deduced from a control experiment. In this control experiment, 1,12-dodecanedioc acid was substituted by 1,6-hexanedioic acid in the synthesis procedure and an amorphous polymer was obtained (data not shown). Clearly, the intensity of this peak was found to be reduced for PXDHC*y* composite that may be caused by the decrease of PXD content. When Fig. 3A and 3B are compared it can be observed that this peak becomes narrow and sharp. Furthermore, the diffraction peak attributed to the HA becomes more visible after extraction, which also can be explained by the decrease of PXD after extraction.

The addition of inorganic filler in polymer matrix could generally influence the behavior of polymer crystallization in two counteracting manners [36]. On one hand, the inorganic particles can hinder the motion of polymer segments during crystallization. On the other hand, physical interaction between inorganic particles and polymer segments enables crystallization occurring already at a higher temperature compared to the bulk material [37]. Polymer crystallinities of PXD and PXDHC*y* were quantified by deconvolution of diffraction pattern [38]. Calculated polymer crystallinity (X_c) of PXD and PXDHC*y* composites before- and after extraction are depicted in Fig. 3D. Although the change in crystallinity (before- and after- extraction) does not occur in a consistent manner, extracted samples show higher degrees of crystallinity than unextracted samples, which can be attributed to hindered crystallization by the soluble content of the reaction

mixture. Generally, the presence of only a small HA content reduced the crystallization of PXD matrix, resulting in a decrease of crystallinity [39]. On the other hand, physical interaction between HA and PXD polymer chain enabled the formation of polymer crystalline structures on the surface of the HA particles. When HA acted as nucleating agent, PXD polymer chain segments crystallized on the surface of HA particles, which may cause the increase in polymer crystallinity [40]. These results are in agreement with similar findings of HA in polymer matrices [37].

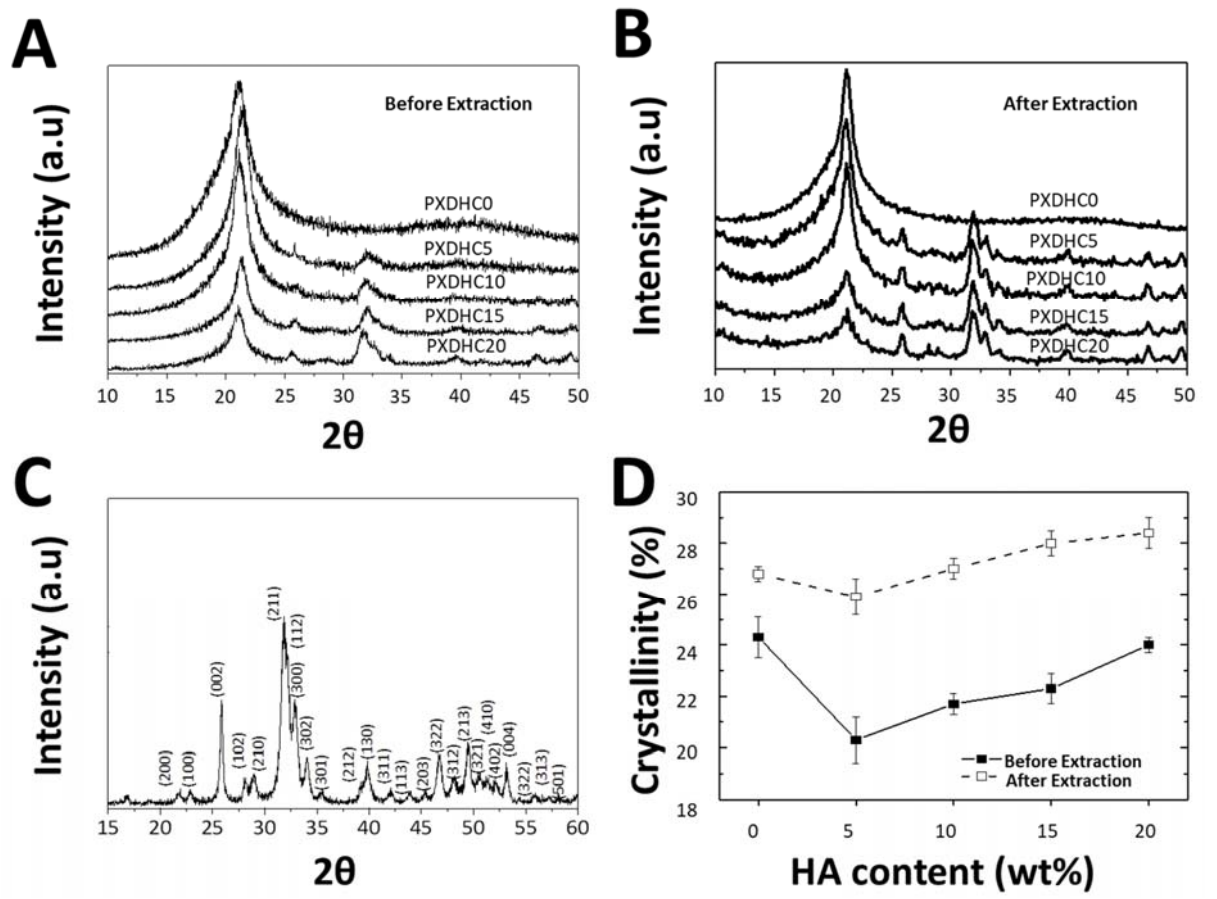

Fig. 3. (A) WAXD patterns of PXD and PXDHC*y* composites before extraction; (B) WAXD patterns of PXD and PXDHC*y* composites after extraction; (C) WAXD pattern of HA; (D) Crystallinity of PXD and PXDHC*y* composites. Solid cubes connected with solid line are the crystallinity before extraction. Hollow cubes connected with dash lines represent the crystallinity after extraction.

The thermal properties of PXD and PXDHC*y* composites were analyzed by means of DSC. In the cooling curves, the crystallization temperatures (T_c) of all PXDHC*y* composites were higher than neat PXD (Fig. 4A). This implies a dominance of the physical interaction between HA and PXD matrix and as a result the PXD matrix is able to crystallize on surface of HA particles at higher temperatures compared to neat PXD. Nucleating effects of HA increased when the HA content within the PXD matrix increased.

In the DSC curves (along heating direction), all PXDHC*y* composites showed higher glass-transition temperature (T_g) and melting-temperatures (T_m) when compared to neat PXD (Fig. 4B). Restriction on micro-Brownian motion of polymer molecular chains caused by the presence of HA particles might be the reason for a higher thermal transition temperature of the polymer/HA composite compared to the neat polymer [41]. Nevertheless, existence of the physical interaction between polymer matrix and HA particles will also provide a higher thermal transition temperature. The T_m of PXDHC*y* composites remained at about 55 °C and did not change when the HA loading increased (Fig. 4B). Obviously, there are two contrary effects caused by HA particles in the polymer matrix. As discussed by Lei and co-workers, inorganic particles may hinder crystallization of a polymer matrix, resulting in reduction of T_m. In contrast, stronger physical interaction within an inorganic/organic matrix could be shown by an incremental change in T_m. Our research indicates a balance between the two counteracting effects caused by addition of HA particles. Under these extraordinary conditions, T_m of the PXDHC*y* composites neither increased nor decreased when the HA content was varied.

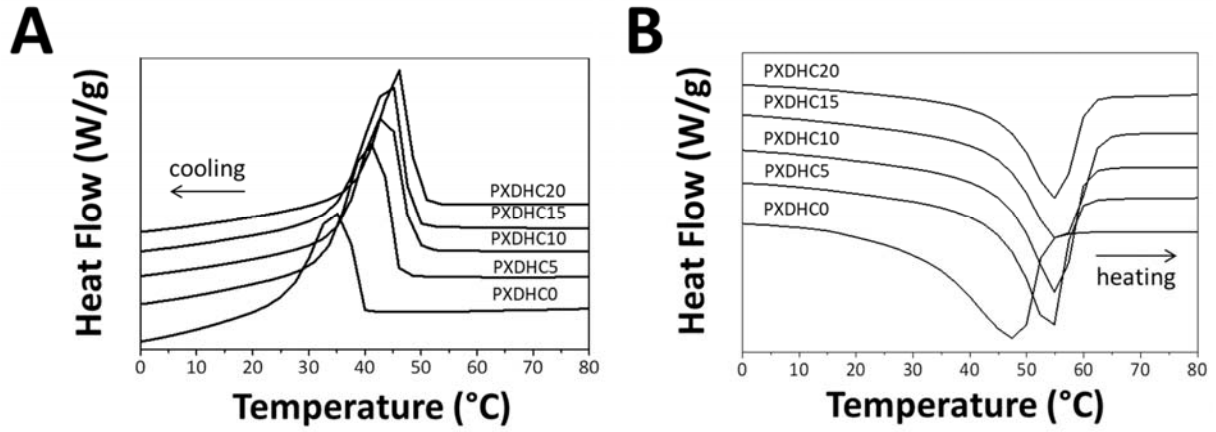

Fig. 4. (A) DSC cooling scans of PXD and PXDHC*y* composites; (B) DSC heating scans of PXD and PXDHC*y* composites.

Tensile tests of PXD and PXDHC*y* composites were performed at 25 °C and 70 °C respectively, and the mechanical properties and typically recorded stress-strain curves are shown in Table 1 and Fig. 5. At ambient temperature, PXD and PXDHC*y* composites behave like thermoplastic materials and undergo permanent yielding as well as stress whitening because of tensile force. Conversely, all samples show elastomeric properties when heated above T_m. In this aspect, elastomers differ considerably from thermoplastics, as the latter will not regain the original shape once stress is removed. Tensile properties of PXDHC0 at low temperature are comparable to other semicrystalline polymers [42]. At both temperatures, PXDHC*y* composites were stiffer when loaded with HA, indicated by increased Young's modulus (*E*), which may suggest good interfacial interaction between the PXD matrix and the embedded HA particles without the need of extra surface treatment. In comparison, other bio-based polymers (*e.g.* PLA and PCL) required surface modification on HA for enhancement of interfacial properties or otherwise, the mechanical properties may not significantly improve [43,44]. Mechanical properties of PXD and PXDHC*y* composites decreased upon heating from 25 °C to 70°C. Taking PXDHC20 as an example, tensile strength and Young's modulus were decreased from 17.0 ± 1.0 MPa to 1.20 ± 0.09 MPa and 508

± 11.3 MPa to 2.90 ± 0.20 MPa while the elongation at break increased from 8.7 ± 1.5 % to 52.0 ± 1.5 %. Though elongation at break of PXD and PXDHC*y* composites are quite low, the stresses at break at room temperature are relatively high, which justifies the proposed application of a shape-memory polymer-based as smart fixation plug where the device needs to sustain high stresses.

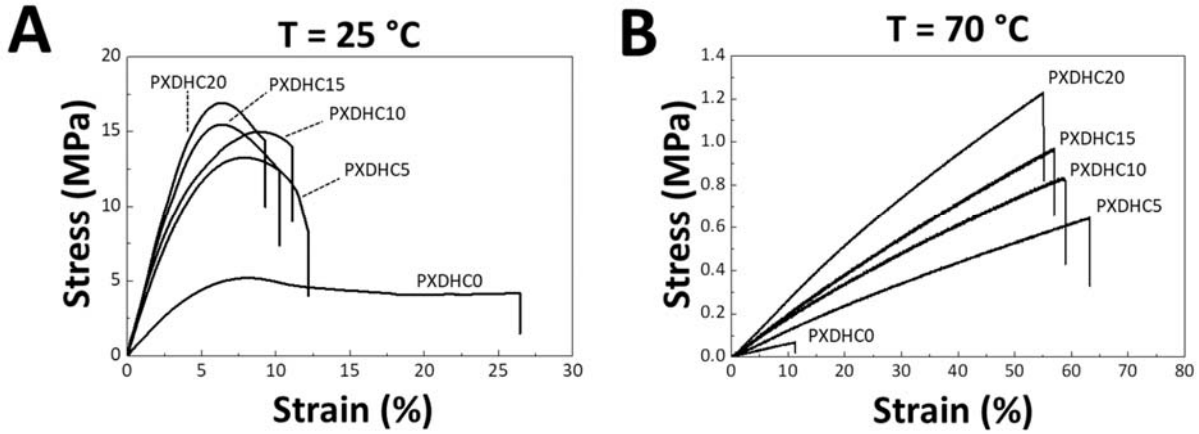

Fig. 5. Stress-strain curves of PXD and PXDHC*y* composites at different temperatures; (A) 25 °C; (B) 70 °C.

FESEM micrographs and EDS particles mappings of the tensile-fracture surface of PXDHC*y* composites with 5, 10, 15, and 20 wt% of HA are shown in Fig. 6. Tensile-fractured surface of the PXDHC*y* samples with 5 wt% and 10 wt% of HA reveal a fractured fibrous texture of the polymer matrix with an overall smooth polymer surface that cover agglomerated HA particles. In contrast, PXDHC*y* samples with 15 wt% and 20 wt% of HA showed a relatively rough surface, suggesting significant adhesion of HA particles to PXD matrix for composites [45]. Particle mapping was performed on PXDHC*y* composites by means of EDS to explore the distribution of calcium (*Ca*) and phosphorus (*P*) as the main components of hydroxyapatite. These particles maps provided visual evidence for a homogenous dispersion of HA particles within PXD

matrix. EDS spectroscopy studies were performed at the same area where the micrographs of FESEM were taken. From the map of elemental distribution, it can be concluded that the physical interface interaction of HA particles and PXD matrix effectively improves the dispersity of HA.

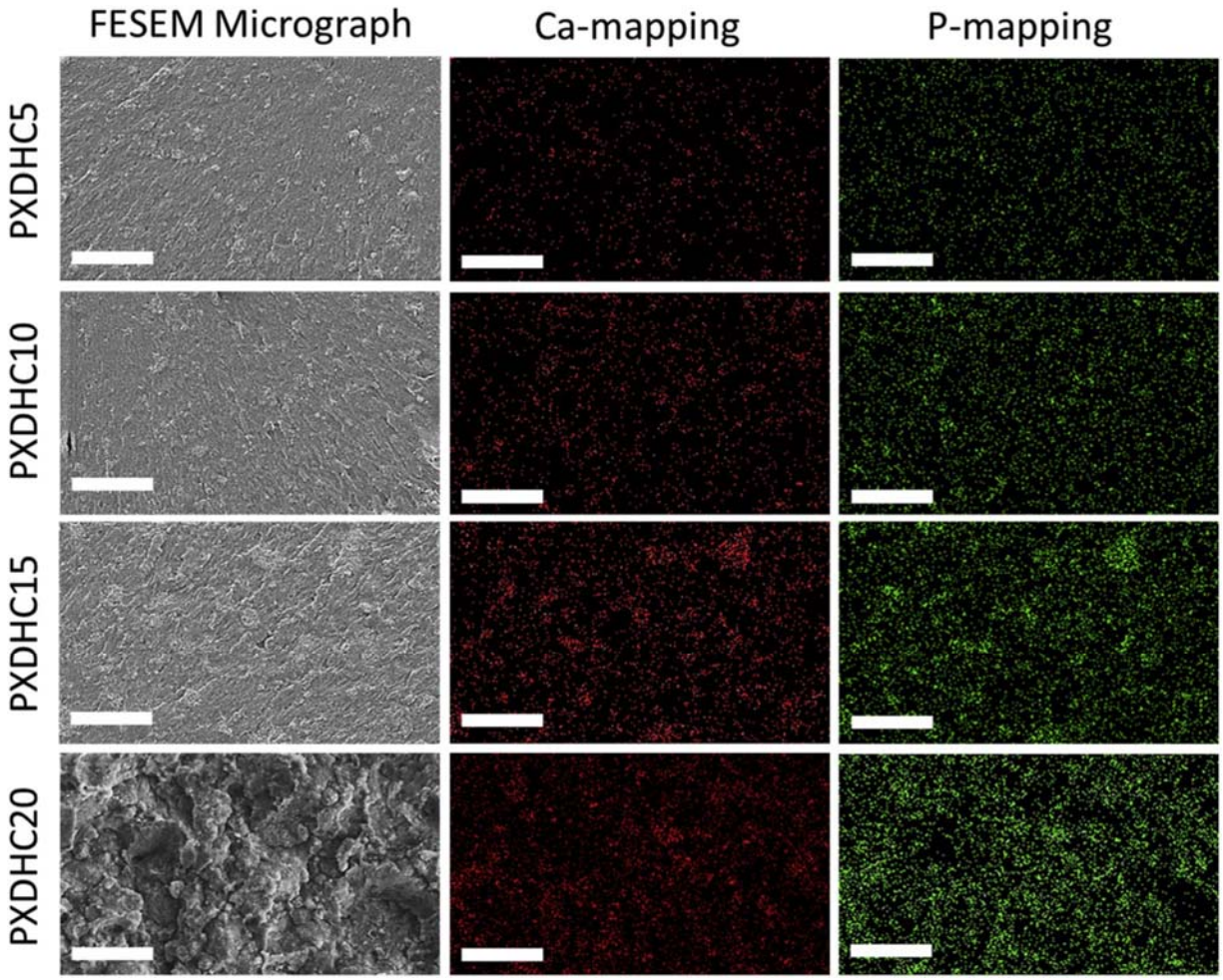

Fig. 6. FESEM micrographs and EDS particles mapping on tensile fracture surface of PXDHC*y* composites. Scale bars represent 50 μm.

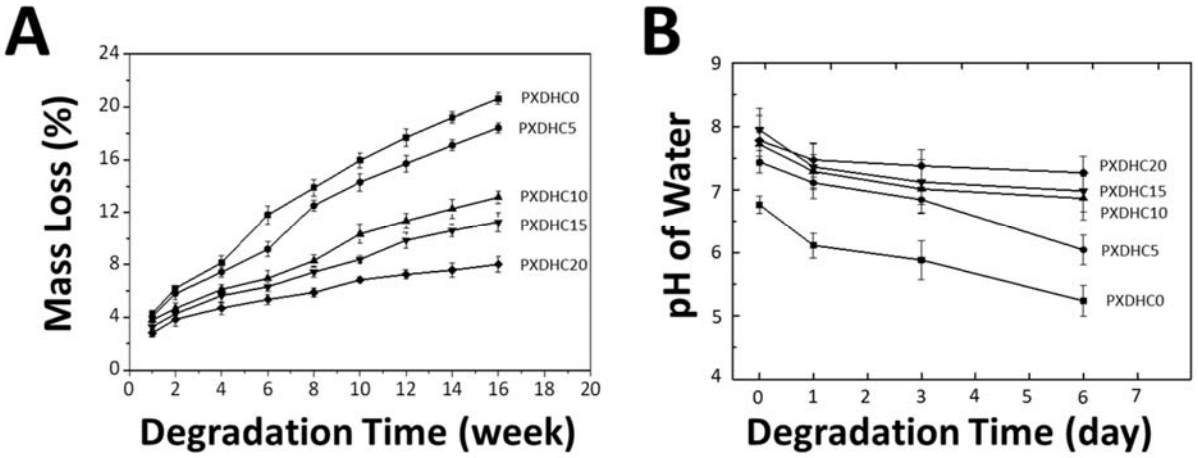

Fig. 7. (A) Mass loss of PXD and PXDHC*y* composites in distilled water at different time intervals; (B) pH of water after immersion of PXD and PXDHC*y* composites at different time intervals.

Fig. 7A shows the percentage of mass loss of PXD and PXDHC*y* composites during incubation in distilled water at room temperature. Distilled water was selected to simulate the hydrolytic degradation of disposed biopolymers by rain on a landfill. It was found that all of the PXD and PXDHC*y* composites were just degraded by immersion in distilled water (eco-friendly disposable bio-based composites). It can be concluded that the degradation of PXD involves three stages, which is similar to thermally crosslinked polyesters [32]. Three stages can be identified in the mass loss profile of PXD during incubation in water. In the first stage, sol content, which is not part of the PXD crosslinked network, degraded in advance of gel content because the sol has short chain molecules resulting a relatively fast mass loss in the earlier stage of degradation (up to week 2). In the second stage, caused by this gain in volume, water will penetrate into sample matrix and mass loss caused by the hydrolysis of ester bonds, gradually reaches an equilibrium plateau (from week 2 to week 6). In the last stage, the gel fraction started to degrade into sol. However, the process took some time and the degradation rate was slow during this stage. When a certain time point is reached, cleavage of bonds of the formerly three-dimensional crosslinked polymer network was completely degraded into a linear polymer chain and subsequent degradation results

in a linear mass loss (after week 6). As stated, the weight loss is due to the aqueous hydrolytic degradation of PXD. The process involved cleavage of ester structures into carboxyl and hydroxyl groups. Cleavage of the ester structures during incubation in water was evidenced by the decrease in pH of the medium caused by the formation of carboxyl groups (Fig. 7B).

Although all of the PXDHC*y* composites degraded in a similar pattern as observed for the degradation of PXD, the degradation rate was affected by the presence of HA particles. PXDHC*y* composites showed slower degradation rate when compared to PXD. This result is in line with the degradation behavior of other polyester/hydroxyapatite composites [36]. The slow degradation of PXDHC*y* composites can be explained by a buffering effect of the HA in the incubation medium [46-48]. In addition, the HA increases crystallinity and semicrystalline materials with a higher crystalline weight fraction are known to degrade slower. As promising green-chemistry material, it may be possible for PXD and PXDHC*y* composites with advanced biodegradability to replace petrol-based materials, thereby to overcome the challenge of disposal and landfill. Unlike PLA (a common known biodegradable polymer) that requires a plethora of requirements to effectively decompose (*e.g*. anaerobic condition, temperature above 60 °C, and presence of microbes) and which are difficult to fulfill in a landfill).

The shape-memory effects of PXD and PXDHC*y* composites were quantified by means of cyclic thermomechanical tests under strain-controlled conditions. PXDHC*y* is a classical thermally-induced shape-memory material, which becomes elastic when heated above T_m of the PXD domains. In this flexible state, a deformation into a new temporary shape can be applied. Cooling of the samples below the crystallization temperature of the PXDHC*y* while load was maintained enabled fixation of the temporary shape. Once the sample is heated above T_m of the PXDHC*y*, shape recovery occurs and sample reverses into its original shape. Fig. 8A shows exemplarily the shape-memory cycles of PXDHC20 from which the shape-fixity ratio (R_f) and

shape-recovery ratio (R_r) were determined, R_f and R_r of the other samples can be assessed from Fig. 8B. As shown in the tensile test results, the presence of HA particles enhanced strain at break of the matrix, suggesting that PXDHC*y* composites can be deformed into temporary shapes, which differ more from the original permanent shape as compared to samples solely from PXD. Fig. 8C illustrates proposed polymer network architecture of PXD in which xylitol acts as net points while 1,12-dodecanedioic acid act as switching segment (crystallizable segment).

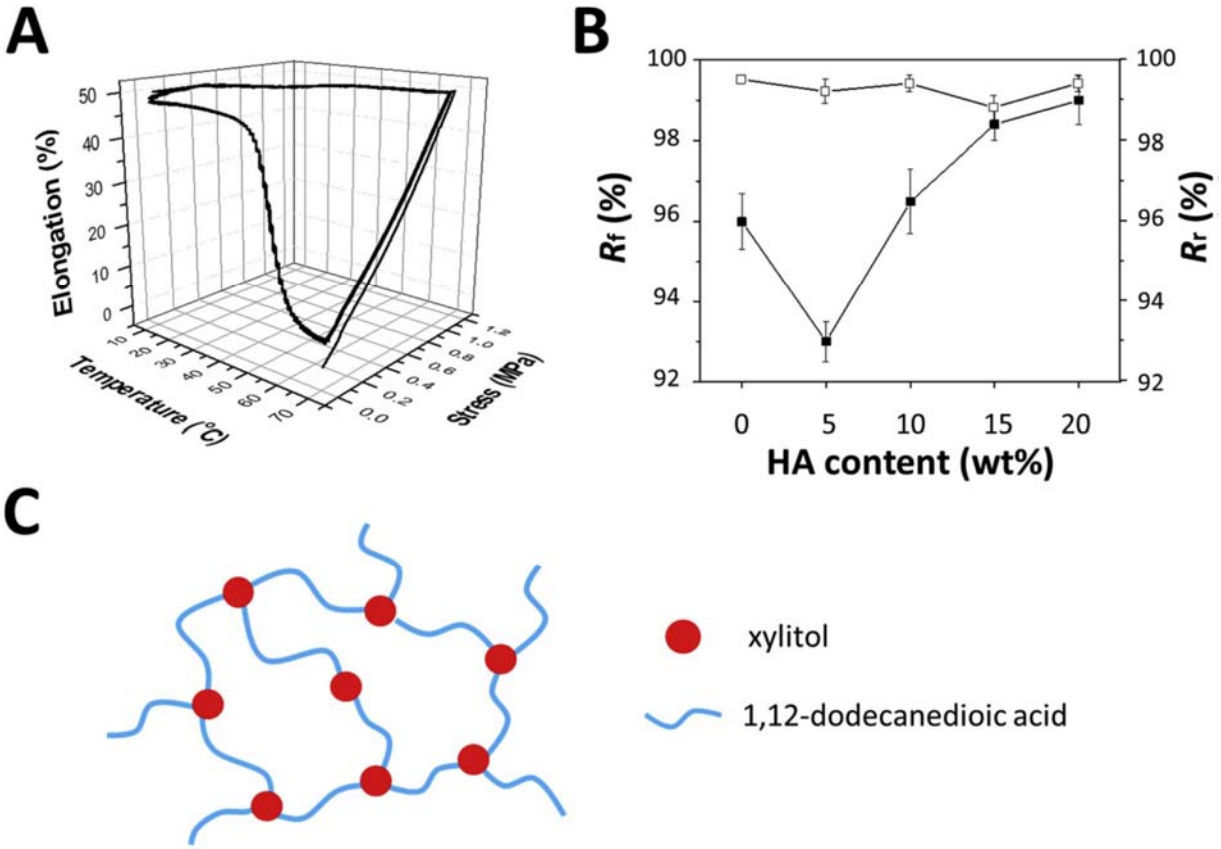

Fig. 8. (A) Results of strain-controlled cyclic thermomechanical test of sample PXDHC20; (B) Shape-memory properties of PXD and PXDHCy composites; (C) Schematic representation of polymer network architecture of PXD.

In the initial experiments, the shape-memory properties of a smart fixation application of this bio-based composite plug for household appliances were investigated. First, the demonstrator

was heated to 70 °C followed by an elongation of about 50 % using a custom-made stainless steel sample extender (Fig. 9A). The deformed prototype was then cooled to room temperature to fix this temporary shape similar to the shape-programming procedure described for the cyclic, thermomechanical investigations. Photographs of the sample in programed shape were taken after 1 hour and 2 years to show short-term and long-term shape fixity of sample PXDHC20. Shape-recovery procedures were conducted by placing the demonstrator (in its temporary shape) into a water bath of 70 °C (Fig. 9B). The fixation capability of the demonstrator was explored in another experiment. The fixation demonstrator was placed at each end into a device consisting of two PMMA blocks each providing an insertion hole. Once both blocks were joined, the shape-memory effect was initiated. Even when a load of 12.5 kg was hung over the lower acrylic block, the fixation device still did not disintegrate and was capable of keeping both parts fixed (Fig. 10). Last by no means least, it is important to mention that the synthesis and fabrication of PXDHC*y* does not involve any harsh solvents or exogenous reaction initiators or catalysts.

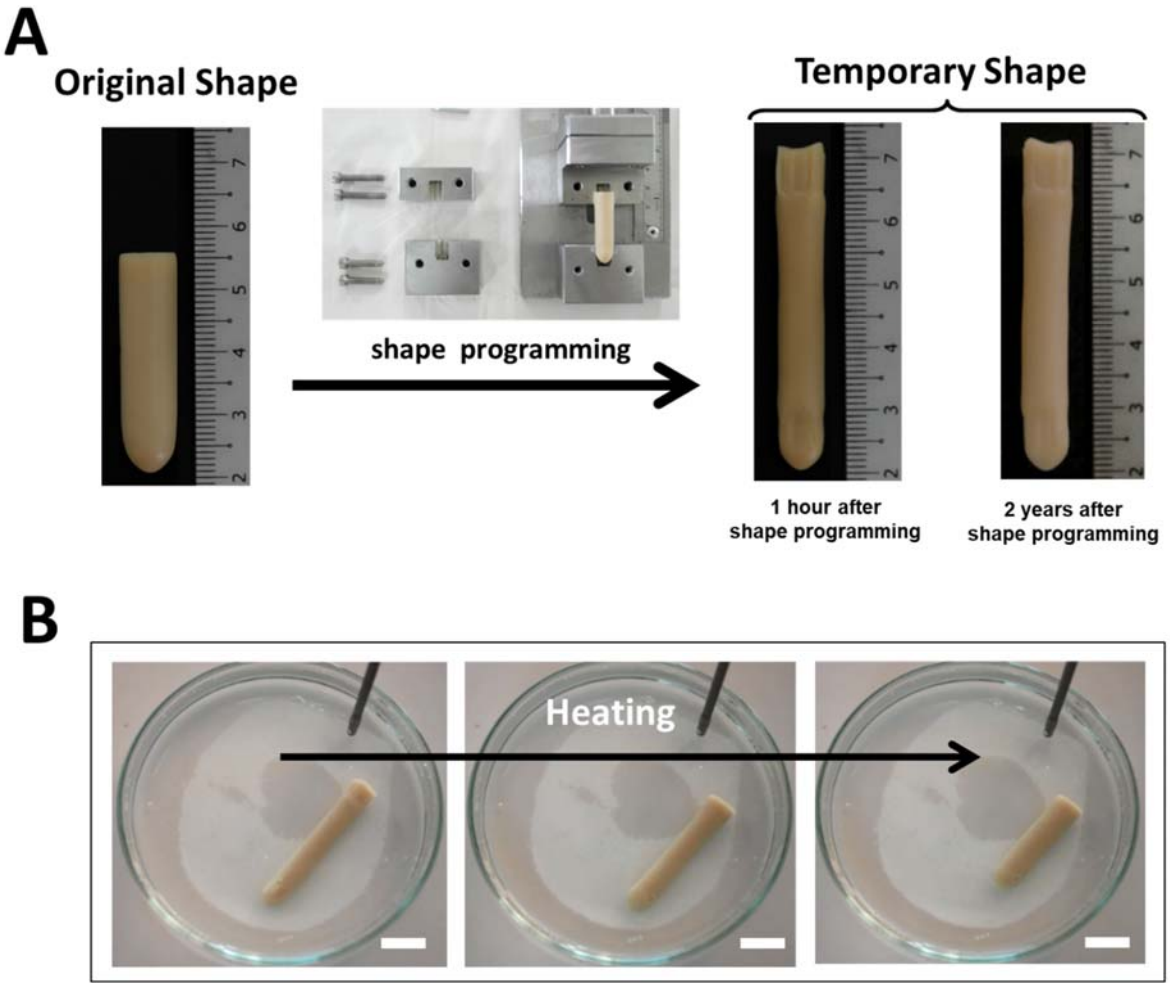

Fig. 9. Proposed application as smart fixation plug. (A) Photographs show programming of sample PXDHC20, short-term shape fixity, and long-term shape fixity of sample in temporary shape. (B) Photographs exhibiting the self-expansion of bio-based composite plug during incubation in distilled water at 70 °C. Scale bars represent 1 cm.

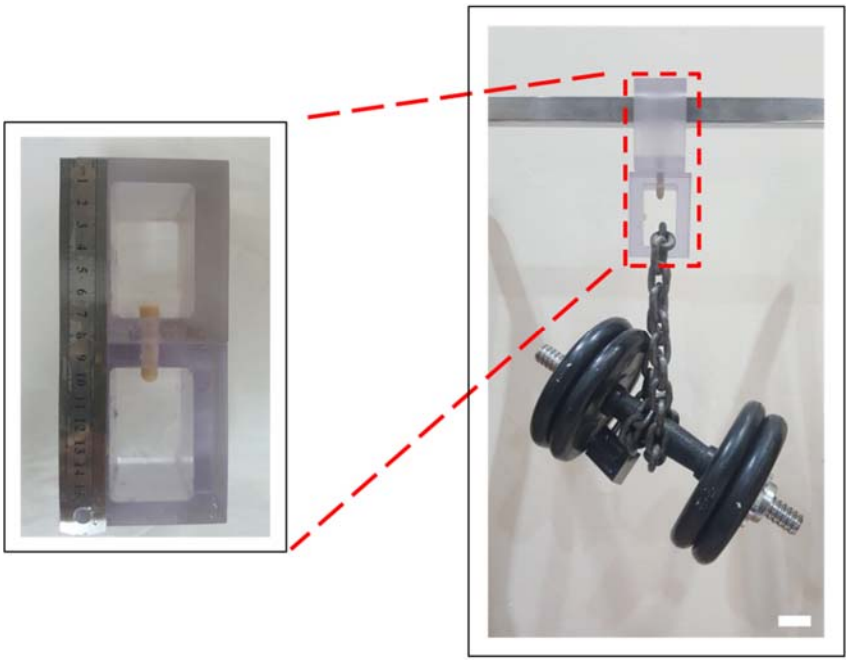

Fig. 10. Demonstration experiment of the bio-based composite in a fixation application, sample PXDHC20 (weight of load is 12.5 kg). Scale bar represents 3 cm.

4. Conclusion

In this work, a new class of bio-based composites was developed from hydroxyapatite, xylitol, and 1,12-dodecanedioic acid. The results indicate two counteracting effects caused by HA addition within the PXD matrix on the structural and thermal properties. All PXDHC*y* bio-based composites and the PXD reference compound showed excellent shape-fixity ratio (R_f) higher than 93% and shape-recovery ratio (R_r) higher than 99%. Results showed all of the PXD and PXDHC composites able to degrade hydrolytically, which can be considered as environmentally friendly materials. A prototype smart fiation plug was demonstrated by using PXDHC20 composite as the material basis. The demonstrator could be plugged into small insertion holes in a compacted temporary shape and then self-expand upon reheating to fix two parts together. The discussed PXDHC*y* bio-based composites were prepared from bio-based feedstocks via a relatively simple method and potential to be used in numerous fixation purposes.

TABLE

Table 1. Physical, thermal, and mechanical properties of PXD and PXDHC*y* composites at 25 °C and 70 °C, respectively

Sample ID[a]	G[b] (%)	Q[b] (%)	T_g[c] (°C)	T_m[c] (°C)	T = 25°C			T = 70 °C			ν[e] (mol/m³)
					σ[d] (MPa)	ε[d] (%)	E[d] (MPa)	σ[d] (MPa)	ε[d] (%)	E[d] (MPa)	
PXDHC0	76.0 ± 0.9	568 ± 14	-1	48	5.7 ± 0.9	26.8 ± 9.9	116.1 ± 16.2	0.05 ± 0.02	11.7 ± 4.2	0.56 ± 0.03	65.4 ± 3.5
PXDHC5	74.2 ± 0.6	545 ± 10	7	55	12.8 ± 2.9	12.8 ± 9.4	367.5 ± 10.1	0.61 ± 0.08	61.6 ± 9.4	1.23 ± 0.15	135.8 ± 16.6
PXDHC10	76.0 ± 1.0	506 ± 13	11	55	15.1 ± 1.2	11.3 ± 2.1	439.5 ± 13.8	0.79 ± 0.08	57.8 ± 7.2	1.82 ± 0.23	187.7 ± 23.7
PXDHC15	77.6 ± 0.4	464 ± 12	14	55	15.8 ± 1.1	10.7 ± 2.2	470.4 ± 18.7	0.92 ± 0.08	57.4 ± 7.6	2.11 ± 0.25	200.7 ± 23.8
PXDHC20	79.4 ± 0.5	446 ± 21	17	55	17.1±1.0	8.7 ± 1.5	507.8 ± 11.3	1.21 ± 0.09	52.0 ± 1.5	2.90 ± 0.20	251.5 ± 17.3

Note

[a] Samples denoted as PXDHC*y*, in which *y* indicates the HA content in wt%.

[b] Gel content (*G*) and degree of swelling (*Q*) of samples determined by swelling experiment in THF at 22 °C.

[c] Glass-transition temperature (T_g) and melting-transition temperature (T_m) were obtained from differential scanning calorimetric thermograms.

[d] Tensile strength (σ), elongation at break (ε), and Young's modulus (*E*) determined by tensile tests at 25 °C and 70 °C.

[e] Network strand density (*v*) calculated from affine theory of rubber elasticity.

AUTHOR INFORMATION

Corresponding Author

* corresponding author: Prof. Dr. Tiefeng Li, Email: litiefeng@zju.edu.cn

* corresponding author: Prof. Dr. Mat Uzir Wahit, Email: r-uzir@utm.my

Author Contributions

[#] These authors contributed equally to this work.

Declaration of competing interest

The authors declare that they have no known competing financial interests or personal relationships that could have appeared to influence the work reported in this paper.

ACKNOWLEDGMENT

This work was supported by the following programs: Research University Grant (GUP tier 1: G.J13000.2545.16H18), Ministry of Higher Education Malaysia (High Centre of Excellence: R.J090301.7846.4J258), UTM Potential Academic Staff Research Grant (PAS grant: Q.J130000.2745.02K42), National Key R&D Program of China 2017YFA0701100, National Natural Science Foundation of China (11822207, U1613202), and programme-oriented funding of the Helmholtz Association. Technical support by Sabine Benner and Karolin Schmälzlin is acknowledged.

REFERENCES

[1] I.S.M. Rafiqul, A.M.M. Sakinah, Processes for the Production of Xylitol—A Review, Food Rev. Int. 29 (2013) 127-156, https://doi.org/10.1080/87559129.2012.714434.

[2] F.O. Ayorinde, F.T. Powers, L.D. Streete, R.L. Shepard, D.N. Tabi, Synthesis of dodecanedioic acid fromvernonia galamensis oil, J. Am. Oil Chem. Soc. 66 (1989) 690-692, https://doi.org/10.1007/bf02669953.

[3] M.S. Shet, C.W. Fisher, P.L. Holmans, R.W. Estabrook, The Omega-Hydroxylation of Lauric Acid: Oxidation of 12-Hydroxylauric Acid to Dodecanedioic Acid by a Purified Recombinant [4] Fusion Protein Containing P450 4A1 and NADPH–P450 Reductase, Arch. Biochem. Biophys. 330 (1996) 199-208, https://doi.org/10.1006/abbi.1996.0243.

[4] J.-W. Song, J.-H. Lee, U.T. Bornscheuer, J.-B. Park, Microbial Synthesis of Medium-Chain α,ω-Dicarboxylic Acids and ω-Aminocarboxylic Acids from Renewable Long-Chain Fatty Acids, Adv. Synth. Catal. 356 (2014) 1782-1788, https://doi.org/10.1002/adsc.201300784.

[5] H. Uyama, M. Kuwabara, T. Tsujimoto, M. Nakano, A. Usuki, S. Kobayashi, Green Nanocomposites from Renewable Resources: Plant Oil−Clay Hybrid Materials, Chem. Mater. 15 (2003) 2492-2494, https://doi.org/10.1021/cm0340227.

[6] H. Fu, Y. Wang, X. Li, W. Chen, Synthesis of vegetable oil-based waterborne polyurethane/silver-halloysite antibacterial nanocomposites, Compos. Sci. Technol. 126 (2016) 86-93, https://doi.org/10.1016/j.compscitech.2016.02.018.

[7] G. Capiel, N.E. Marcovich, M.A. Mosiewicki, Shape memory polymer networks based on methacrylated fatty acids, Eur. Polym. J. 116 (2019) 321-329, https://doi.org/10.1016/j.eurpolymj.2019.04.023.

[8] Y. Feng, Y. Hu, L. Man, T. Yuan, C. Zhang, Z. Yang, Biobased thiol-epoxy shape memory networks from gallic acid and vegetable oils, Eur. Polym. J. 112 (2019) 619-628, https://doi.org/10.1016/j.eurpolymj.2018.10.025.

[9] J.P. Bruggeman, C.J. Bettinger, C.L.E. Nijst, D.S. Kohane, R. Langer, Biodegradable Xylitol-Based Polymers, Adv. Mater. 20 (2008) 1922-1927, https://doi.org/10.1002/adma.200702377.

[10] P. Niedermann, G. Szebényi, A. Toldy, Characterization of high glass transition temperature sugar-based epoxy resin composites with jute and carbon fibre reinforcement, Compos. Sci. Technol. 117 (2015) 62-68, https://doi.org/10.1016/j.compscitech.2015.06.001

[11] C. Véchambre, L. Chaunier, D. Lourdin, Novel Shape-Memory Materials Based on Potato Starch, Macromol. Mater. Eng. 295 (2010) 115-122, https://doi.org/10.1002/mame.200900191.

[12] M. Soheilmoghaddam, G. Sharifzadeh, R.H. Pour, M.U. Wahit, W.T. Whye, X.Y. Lee, Regenerated cellulose/β-cyclodextrin scaffold prepared using ionic liquid, Mater. Lett. 135 (2014) 210-213, https://doi.org/10.1016/j.matlet.2014.07.169.

[13] M. Soheilmoghaddam, H. Adelnia, G. Sharifzadeh, M.U. Wahit, T.W. Wong, A. Ali Yussuf, Bionanocomposite regenerated cellulose/single-walled carbon nanotube films prepared using ionic liquid solvent, Cellulose 24 (2017) 811-822, https://doi.org/10.1007/s10570-016-1151-3.

[14] T. Saito, R.H. Brown, M.A. Hunt, D.L. Pickel, J.M. Pickel, J.M. Messman, F.S. Baker, M. Keller, A.K. Naskar, Turning renewable resources into value-added polymer: development of lignin-based thermoplastic, Green Chem. 14 (2012) 3295-3303, https://doi.org/10.1039/C2GC35933B.

[15] D. Kai, H.M. Chong, L.P. Chow, L. Jiang, Q. Lin, K. Zhang, H. Zhang, Z. Zhang, X.J. Loh, Strong and biocompatible lignin /poly (3-hydroxybutyrate) composite nanofibers, Compos. Sci. Technol. 158 (2018) 26-33, https://doi.org/10.1016/j.compscitech.2018.01.046.

[16] C. Zhang, T.F. Garrison, S.A. Madbouly, M.R. Kessler, Recent advances in vegetable oil-based polymers and their composites, Prog. Polym. Sci. 71 (2017) 91-143, https://doi.org/10.1016/j.progpolymsci.2016.12.009.

[17] H. Qiu, J. Yang, P. Kodali, J. Koh, G.A. Ameer, A citric acid-based hydroxyapatite composite for orthopedic implants, Biomaterials 27 (2006) 5845-5854, https://doi.org/10.1016/j.biomaterials.2006.07.042.

[18] J. Pietrasik, K. Szustakiewicz, M. Zaborski, K. Haberko, Hydroxyapatite: An Environmentally Friendly Filler for Elastomers, Mol. Cryst. Liq. Cryst. 483 (2008) 172-178, https://doi.org/10.1080/15421400801904880.

[19] P. Shi, M. Liu, F. Fan, C. Yu, W. Lu, M. Du, Characterization of natural hydroxyapatite originated from fish bone and its biocompatibility with osteoblasts, Mater. Sci. Eng. C 90 (2018) 706-712, https://doi.org/10.1016/j.msec.2018.04.026.

[20] S.-L. Bee, Z.A.A. Hamid, Characterization of chicken bone waste-derived hydroxyapatite and its functionality on chitosan membrane for guided bone regeneration, Compos. Part B 163 (2019) 562-573, https://doi.org/10.1016/j.compositesb.2019.01.036.

[21] M. Behl, M.Y. Razzaq, A. Lendlein, Multifunctional Shape-Memory Polymers, Adv. Mater. 22 (2010) 3388-3410, https://doi.org/10.1002/adma.200904447.

[22] P.M. Cook, R.M. Halperin, Arthur Charlesby—His impact on creating a new industry, Radiat. Phys. Chem. 51 (1998) 7-8, https://doi.org/10.1016/S0969-806X(97)00251-X.

[23] A.Lendlein, M. Behl, Shape-Memory Polymers for Biomedical Applications, Adv. Sci. Technol. 54 (2009) 96-102, https://doi.org/10.4028/www.scientific.net/AST.54.96.

[24] C.Löwenberg, M. Balk, C. Wischke, M. Behl, A. Lendlein, Shape-Memory Hydrogels: Evolution of Structural Principles To Enable Shape Switching of Hydrophilic Polymer Networks, Acc. Chem. Res. 50 (2017) 723-732, https://doi.org/10.1021/acs.accounts.6b00584.

[25] T.-W. Wong, J. Wu, M. Yang, M.R. Abdul Kadir, M.U. Wahit, Q. Zhao, Multifunctional shape-memory foams with highly tunable properties via organo-phase cryo-polymerization, J. Mater. Chem. A 5 (2017) 9793-9800, https://doi.org/10.1039/C7TA01661A.

[26] W. Cai, L. Liu, Shape-memory effect of poly (glycerol–sebacate) elastomer, Mater. Lett. 62 (2008) 2171-2173, https://doi.org/10.1016/j.matlet.2007.11.042.

[27] M.C. Serrano, L. Carbajal, G.A. Ameer, Novel Biodegradable Shape-Memory Elastomers with Drug-Releasing Capabilities, Adv. Mater. 23 (2011) 2211-2215, https://doi.org/10.1002/adma.201004566.

[28] T.W. Wong, M.U. Wahit, M.R. Abdul Kadir, M. Soheilmoghaddam, H. Balakrishnan, A novel poly(xylitol-co-dodecanedioate)/hydroxyapatite composite with shape-memory behaviour, Mater. Lett. 126 (2014) 105-108, https://doi.org/10.1016/j.matlet.2014.04.020.

[29] S.-L. Liang, W.D. Cook, G.A. Thouas, Q.-Z. Chen, The mechanical characteristics and in vitro biocompatibility of poly(glycerol sebacate)-Bioglass® elastomeric composites, Biomaterials 31 (2010) 8516-8529, https://doi.org/10.1016/j.biomaterials.2010.07.105.

[30] W. Wagermaier, K. Kratz, M. Heuchel, A. Lendlein, Characterization Methods for Shape-Memory Polymers, Adv. Polym. Sci. 226 (2010) 97-145, https://doi.org/10.1007/12_2009_25.

[31] I. Djordjevic, N.R. Choudhury, N.K. Dutta, S. Kumar, Synthesis and characterization of novel citric acid-based polyester elastomers, Polymer 50 (2009) 1682-1691, https://doi.org/10.1016/j.polymer.2009.01.045.

[32] L. Lei, T. Ding, R. Shi, Q. Liu, L. Zhang, D. Chen, W. Tian, Synthesis, characterization and in vitro degradation of a novel degradable poly((1,2-propanediol-sebacate)-citrate) bioelastomer, Polym. Degrad. Stabil. 92 (2007) 389-396, https://doi.org/10.1016/j.polymdegradstab.2006.12.004.

[33] K.-W. Lee, S. Wang, M.J. Yaszemski, L. Lu, Physical properties and cellular responses to crosslinkable poly(propylene fumarate)/hydroxyapatite nanocomposites, Biomaterials 29 (2008) 2839-2848, https://doi.org/10.1016/j.biomaterials.2008.03.030.

[34] I.S. Elashmawi, H.E. Abdel Baieth, Spectroscopic studies of hydroxyapatite in PVP/PVA polymeric matrix as biomaterial, Curr. Appl. Phys. 12 (2012) 141-146, https://doi.org/10.1016/j.cap.2011.05.011.

[35] W. Guo, J. Liu, P. Zhang, L. Song, X. Wang, Y. Hu, Multi-functional hydroxyapatite/polyvinyl alcohol composite aerogels with self-cleaning, superior fire resistance and low thermal conductivity, Compos. Sci. Technol. 158 (2018) 128-136, https://doi.org/10.1016/j.compscitech.2018.01.020.

[36] L. Lei, L. Li, L. Zhang, D. Chen, W. Tian, Structure and performance of nano-hydroxyapatite filled biodegradable poly((1,2-propanediol-sebacate)-citrate) elastomers, Polym. Degrad. Stabil. 94 (2009) 1494-1502, https://doi.org/10.1016/j.polymdegradstab.2009.04.034.

[37] S. Wang, D.H.R. Kempen, M.J. Yaszemski, L. Lu, The roles of matrix polymer crystallinity and hydroxyapatite nanoparticles in modulating material properties of photo-crosslinked composites and bone marrow stromal cell responses, Biomaterials 30 (2009) 3359-3370, https://doi.org/10.1016/j.biomaterials.2009.03.015.

[38] B. Guo, Y. Chen, Y. Lei, L. Zhang, W.Y. Zhou, A.B.M. Rabie, J. Zhao, Biobased Poly(propylene sebacate) as Shape Memory Polymer with Tunable Switching Temperature for Potential Biomedical Applications, Biomacromolecules 12 (2011) 1312-1321, https://doi.org/10.1021/bm2000378.

[39] X. Zhang, Y.-B. Li, Y. Zuo, G.-Y. Lv, Y.-H. Mu, H. Li, Morphology, hydrogen-bonding and crystallinity of nano-hydroxyapatite/polyamide 66 biocomposites, Compos. Part A 38 (2007) 843-848, https://doi.org/10.1016/j.compositesa.2006.08.002.

[40] A. Sonseca, L. Peponi, O. Sahuquillo, J.M. Kenny, E. Giménez, Electrospinning of biodegradable polylactide/hydroxyapatite nanofibers: Study on the morphology, crystallinity structure and thermal stability, Polym. Degrad. Stabil. 97 (2012) 2052-2059, https://doi.org/10.1016/j.polymdegradstab.2012.05.009.

[41] S. Zhou, X. Zheng, X. Yu, J. Wang, J. Weng, X. Li, B. Feng, M. Yin, Hydrogen Bonding Interaction of Poly(d,l-Lactide)/hydroxyapatite Nanocomposites, Chem. Mater. 19 (2007) 247-253, https://doi.org/10.1021/cm0619398.

[42] L. Wu Xue, M. Huang Wei, B. Lu Hai, C. Wang Chang, P. Cui Hai, Characterization of polymeric shape memory materials, J. Polym. Eng. 37 (1)(2017) 1-20, https://doi.org/10.1515/polyeng-2015-0370.

[43] J. Li, X.L.Lu, Y.F. Zheng, Effect of surface modified hydroxyapatite on the tensile property improvement of HA/PLA composite, Appl. Surf. Sci. 255 (2008) 494-497, https://doi.org/10.1016/j.apsusc.2008.06.067.

[44] S. Rakmae, Y. Ruksakulpiwat, W. Sutapun, N. Suppakarn, Effect of silane coupling agent treated bovine bone based carbonated hydroxyapatite on in vitro degradation behavior and bioactivity of PLA composites, Mater. Sci. Eng. C 32 (2012) 1428-1436, https://doi.org/10.1016/j.msec.2012.04.022.

[45] S.E. Petricca, K.G. Marra, P.N. Kumta, Chemical synthesis of poly(lactic-co-glycolic acid)/hydroxyapatite composites for orthopaedic applications, Acta Biomater. 2 (2006) 277-286, https://doi.org/10.1016/j.actbio.2005.12.004.

[46] W. Heidemann, S. Jeschkeit, K. Ruffieux, J.H. Fischer, M. Wagner, G. Krüger, E. Wintermantel, K.L. Gerlach, Degradation of poly(d,l)lactide implants with or without addition of calciumphosphates in vivo, Biomaterials 22 (2001) 2371-2381, https://doi.org/10.1016/S0142-9612(00)00424-5

[47] T. Niemelä, Effect of β-tricalcium phosphate addition on the in vitro degradation of self-reinforced poly-l,d-lactide, Polym. Degrad. Stabil. 89 (2005) 492-500, https://doi.org/10.1016/j.polymdegradstab.2005.02.003.

[48] L.M. Ehrenfried, D. Farrar, R.E. Cameron, Degradation Properties of Co-Continuous Calcium−Phosphate−Polyester Composites, Biomacromolecules 10 (2009) 1976-1985, https://doi.org/10.1021/bm900397d.

For Graphical Abstract use only

Bio-based Composite from Plant Based Precursors and Hydroxyapatite with Shape-Memory Capability

Tuck-Whye Wong,[a,d,#] Marc Behl,[b,#] Noor Izyan Syazana Mohd Yusoff,[c] Tiefeng Li,[a,*] Mat Uzir Wahit,[c,*] Ahmad Fauzi Ismail,[d] Qian Zhao,[e] and Andreas Lendlein[b]

[#] These authors contributed equally to this work.

* Corresponding author.